

# 光学学报

## 用于悬浮光力系统的低噪声四象限探测器研究

王颖颖<sup>1</sup>, 何沛彤<sup>1</sup>, 梁韬<sup>1</sup>, 高晓文<sup>1\*</sup>, 蒋静<sup>2</sup>, 陈杏藩<sup>2</sup>, 胡慧珠<sup>1,2\*\*</sup>

<sup>1</sup>之江实验室量子传感研究中心, 浙江杭州 310023;

<sup>2</sup>浙江大学光电科学与工程学院, 浙江杭州 310027

**摘要** 悬浮光力系统由于其出色的探测性能, 已成为精密测量领域的研究热点。目前悬浮光力系统的探测方案主要包括平衡探测器方案和四象限探测器方案。平衡探测器噪声性能优越, 但单个探测器只能测量一个方向的悬浮微粒位移信息, 探测系统复杂。四象限探测器方案仅使用单个探测器即可同时探测微粒的三轴位移信息, 探测系统简单, 但噪声性能较差。本文根据悬浮光力系统的需求, 设计了一种四象限探测器, 实现了  $10^5$  量级跨阻增益, 电学噪声达到商用平衡探测器水平, 共模抑制比优于 45 dB(50~250 kHz), 且入射光功率大于 1 mW 时, 噪声性能只受散粒噪声限制。实验表明, 该四象限探测器方案可替代平衡探测器方案, 使探测系统小型化, 并能很好地满足高探测灵敏度的需求。

**关键词** 探测器; 光电探测器; 悬浮光力系统; 噪声分解; 共模抑制

中图分类号 TN29

文献标志码 A

DOI: 10.3788/AOS222013

### 1 引言

近年来, 利用光镊技术悬浮微纳谐振子成为物理学的热点<sup>[1-2]</sup>。悬浮光力系统避免了机械支撑带来的损耗与噪声, 具有超高的探测灵敏度<sup>[3-6]</sup>, 在极弱力测量<sup>[6-10]</sup>、加速度测量<sup>[9,11-12]</sup>、重力测量<sup>[13-14]</sup>等精密测量领域取得了多个技术突破, 是基础物理研究的理想平台。悬浮光力系统的核心是通过探测捕获微粒的相对位置变化来获取微粒的受力信息, 其中捕获微粒的位置信息一般是通过微粒散射光与捕获光相互干涉形成的探测光得到的, 因此光源噪声、探测电学噪声等引起的位置探测误差是直接影响系统探测灵敏度的重要因素之一。

目前, 悬浮光力系统的微粒位移探测方案主要包括平衡探测器(BPD)方案和四象限探测器(QPD)方案。BPD 的电流差分结构能够去除共模直流信号, 仅将包含位移信息的交流光电流(一般比直流信号小三个数量级)放大, 因此信噪比较高。由于其优秀的探测性能, BPD 方案能够实现高探测灵敏度, 已被广泛应用于悬浮光力系统<sup>[6,15-18]</sup>中, 并且能够实现量子基态冷却。但该方案需要将探测光分成三束(X、Y、Z 三轴)功率相近的光, 并使用 3 个 BPD 分别进行探测, 探测系统复杂, 不利于小型化。

相比 BPD 方案, QPD 方案弥补了其缺陷, 仅使用单个探测器即可同时获得微粒的三轴位移信息。早在

2004 年, 欧洲分子生物学实验室的 Tischer 等<sup>[19]</sup>就将 QPD 芯片结合前置放大器用于液体光镊中的微粒位移探测。之后在 2015 年, 内华达大学 Ranjit 等<sup>[20]</sup>将 QPD 用于悬浮光力系统中微粒的位移测量和力探测。次年, 该课题组利用 QPD 方案实现了  $1.63 \times 10^{-18} \text{ N/Hz}^{1/2}$  的力探测灵敏度<sup>[10]</sup>。近十年中, 其他课题组也将 QPD 方案用于悬浮光力系统的位移探测<sup>[7-8,21-22]</sup>。然而, 商用 QPD 没有对总光功率变化的探测(Z 轴)进行共模抑制, 并且缺少电流差分结构, 捕获光干扰项生成的光电流直流分量会与位移信号一起放大, 导致其噪声性能较差, 难以达到 BPD 的水平。此外, 商用 QPD 的带宽、饱和光功率等指标也不能完全满足悬浮光力系统的需求, 限制了悬浮光力系统的探测灵敏度。为弥补商用 QPD 的不足, 2017 年苏黎世联邦理工学院的 Lukas Novotny 课题组对 QPD 进行了自研, 实现了对 Z 轴的共模抑制和 50 mW 的高饱和光功率, 但并未对电学噪声进行改善, 最终实现的电学噪声功率谱密度(PSD)相比商用 BPD 高两个数量级, 探测性能提高有限<sup>[23]</sup>。在 2022 年对悬浮微粒冷却的最新研究中, Vijayan 等<sup>[24]</sup>仅将自研 QPD 用于反馈控制环路外的信号观测。

为了提升 QPD 方案的噪声性能, 本文提出了一种有源电流滤波方案, 可在不影响四象限响应参数的前提下将光电流分解, 并且对四象限的响应系数进行校

收稿日期: 2022-11-18; 修回日期: 2022-12-25; 录用日期: 2023-02-21; 网络首发日期: 2023-03-09

基金项目: 国家自然科学基金面上项目(62075193)、之江实验室科研攻关重大项目(2019MB0AD01)、之江实验室自立创新项目(2021MB0AL02)

通信作者: \*gaoxw@zhejianglab.com; \*\*huhuizhu2000@zju.edu.cn

准。最终实现QPD的电学噪声性能达到商用BPD水平,共模抑制比(CMRR)优于45 dB(50~250 kHz),在入射光功率大于1 mW时,噪声性能仅受散粒噪声限制。本文所提出的QPD方案已成功应用于悬浮光力系统进行极弱力传感,简化了探测系统,同时实现了 $4.34 \times 10^{-21}$  N/Hz<sup>1/2</sup>的力学探测灵敏度<sup>[25]</sup>,为小型化高灵敏度探测开辟了新的道路。

## 2 原理

### 2.1 探测系统噪声模型

基于BPD和基于QPD的悬浮光力探测系统示意

图分别如图1(a)和图1(b)所示,图中 $I_{\text{shot}}$ 、 $I_{\text{RIN}}$ 分别为光散粒噪声和相对强度噪声引起的电流噪声, $C_D$ 、 $R_D$ 分别为光电二极管的结电容和分流电阻, $I_s$ 为暗电流, $C_{\text{in}}$ 、 $V_{\text{ni}}$ 、 $I_{\text{ni}}$ 分别为运算放大器的等效输入电容、等效输入电压噪声和等效输入电流噪声。为了获得较好的噪声性能,探测方案通常采用差分探测。探测系统的噪声模型如图1(c)所示,探测系统噪声主要来源于光源噪声和电学噪声。光源噪声主要包括光散粒噪声和光源相对强度噪声(RIN),其中RIN为共模噪声。来自光源的噪声经差分探测器光电转换,在跨阻输出端的噪声功率谱密度表达式为

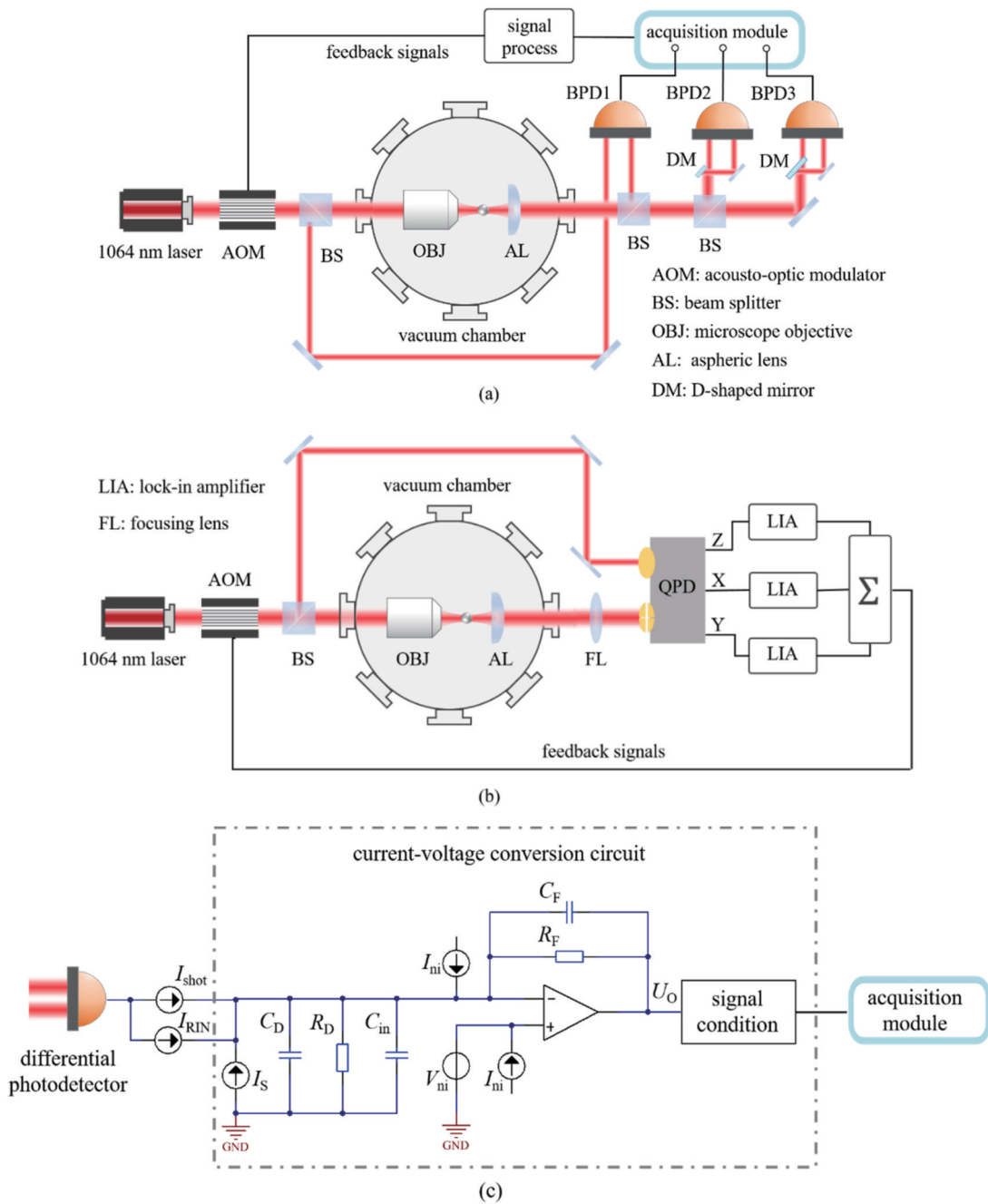


图1 悬浮光力探测系统示意图。(a) BPD方案;(b) QPD方案;(c)噪声模型

Fig. 1 Schematic of levitated optomechanical detection system. (a) BPD scheme; (b) QPD scheme; (c) noise model

$$D_{\text{shot}} = 2e\bar{P}\eta Z^2, \quad (1)$$

$$D_{\text{RIN}} = 10^{-\frac{N_{\text{RIN}} - N_{\text{CMRR}}}{10}} \bar{P}^2 \eta^2 Z^2, \quad (2)$$

式中: $D_{\text{shot}}$ 为散粒噪声在跨阻输出端表现的功率谱密度; $D_{\text{RIN}}$ 为相对强度噪声在跨阻输出端表现的功率谱密度; $e$ 为元电荷; $\bar{P}$ 为平均入射光功率; $\eta$ 为光电二极管的响应度; $N_{\text{RIN}}$ 为光源相对强度噪声; $N_{\text{CMRR}}$ 为差分探测系统的共模抑制比; $Z$ 为光电探测器的等效增益。

除了光源噪声外,探测系统输出信号中还混有较为复杂的电学噪声,主要来源于光电二极管和跨阻放大电路。根据图1(c)的噪声模型,可获得各电学噪声源在跨阻输出端呈现的噪声功率谱密度<sup>[26]</sup>。由于探测器光电二极管的分流电阻一般在几十MΩ量级,暗电流在nA量级,所以光电二极管自身的热噪声和散粒噪声的影响可忽略。选用fA/√Hz量级低电流噪声的FET输入运算放大器,可以忽略运算放大器输入电流噪声的影响。对于悬浮光力探测系统而言,总电学噪声功率谱密度 $D_e$ 由跨阻运算放大器的等效输入电压噪声和反馈电阻热噪声主导。

由各噪声源在跨阻输出端的表现可知,探测系统的总噪声功率谱密度 $D_n$ 可以表示为 $\bar{P}$ 的函数,即 $D_n = D_{\text{RIN}} + D_{\text{shot}} + D_e = K_{\text{RIN}}\bar{P}^2 + K_{\text{shot}}\bar{P} + K_e$ , $K_{\text{RIN}}$ 、 $K_{\text{shot}}$ 和 $K_e$ 分别为光相对强度噪声、光散粒噪声和电学噪声的常系数。在探测系统中测量一组不同入射光功率 $\bar{P}$ 对应的系统总噪声功率谱密度 $D_n$ ,通过最小二乘法拟合得到系数 $K_{\text{RIN}}$ 、 $K_{\text{shot}}$ 和 $K_e$ ,即可计算不同 $\bar{P}$ 时,探测系统中各噪声成分的占比。

目前市面上有多款商用BPD(索雷博、滨松光子等)的基础指标(波长范围、带宽、增益)满足悬浮光力系统的需求,本文从中挑选了索雷博公司的PDB450C-AC型平衡探测器进行噪声分解测试。与其他符合指标的商业BPD产品相比,这款产品的噪声性能更为优越。其饱和功率为1mW,实测1064nm处的响应度为0.8 A/W,增益档位选用10<sup>5</sup>。在悬浮光力系统Y轴位移方向上测量该BPD在差分(DIF)探测以及挡住其中一个光电二极管单端(SE)探测时,不同

$\bar{P}$ (单个光电二极管平均入射光功率)对应的总噪声功率谱密度 $D_n$ ,拟合结果如图2所示。

根据拟合结果计算得到的 $D_{\text{RIN}}$ 、 $D_{\text{shot}}$ 和 $D_e$ 如表1所示。由表1可知,当 $\bar{P}$ 较小时,散粒噪声为主要噪声源,当 $\bar{P}$ 增大至0.32 mW时,单端探测的RIN逐渐成为主要噪声源,通过差分探测手段可以将RIN抑制到低于单端探测时的20 dB以上,因此提高探测系统的共模抑制比是减小RIN影响的有效手段。探测器转换的信号幅度、散粒噪声的噪声功率谱密度均与入射光功率线性正相关,因此提高入射光功率是提升散粒噪声部分信噪比的主要方式。对于电学噪声,增大探测器的第一级跨阻增益可以优化电学噪声,一方面,反馈电阻热噪声部分的信噪比与反馈电阻的阻值成正相关,另一方面,第一级跨阻放大可以在不引入过多噪声的情况下放大信号。由于BPD的电流差分结构,其第一级跨阻增益不受捕获光造成的高直流量限制,从表1拟合的电学噪声 $D_e$ 可知,BPD的电学噪声远低于散粒噪声基准。

据上述分析,为了在简化探测系统的同时,获得不弱于商用BPD的性能,对用于悬浮光力探测系统的QPD提出以下设计指标:可以接收10 mW以上的信

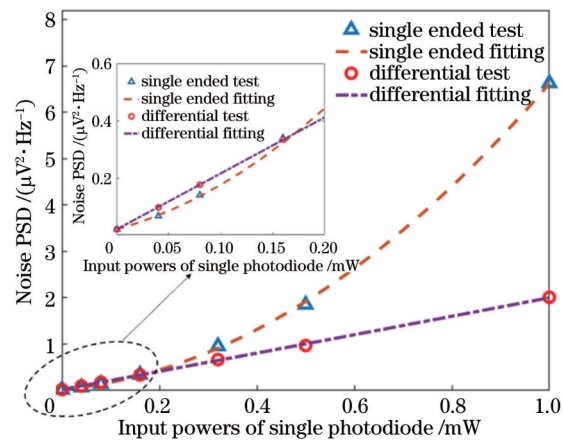


图2 单端探测和差分探测的噪声功率谱密度拟合

Fig. 2 Fitting of noise PSD for single ended test and differential test

表1 由拟合结果得到的BPD探测系统在不同入射光功率时的噪声分解

Table 1 Noise decomposition of BPD detection system at different input optical powers obtained from fitting results

$\bar{P}$ / mW	Test $D_n$ / (dBV <sup>2</sup> ·Hz <sup>-1</sup> )		Fitting $D_n$ / (dBV <sup>2</sup> ·Hz <sup>-1</sup> )		Fitting $D_{\text{RIN}}$ / (dBV <sup>2</sup> ·Hz <sup>-1</sup> )		Fitting $D_{\text{shot}}$ / (dBV <sup>2</sup> ·Hz <sup>-1</sup> )		Fitting $D_e$ / (dBV <sup>2</sup> ·Hz <sup>-1</sup> )	
	SE	DIF	SE	DIF	SE	DIF	SE	DIF	SE	DIF
0	-137.0	-137.0	-137.0	-137.0	0	0	0	0	-137.0	-137.0
0.04	-131.8	-130.2	-131.6	-130.1	-140.5	-164.4	-134.0	-131.1	-137.0	-137.0
0.08	-128.5	-127.6	-128.7	-127.5	-134.5	-158.4	-131.0	-128.1	-137.0	-137.0
0.16	-124.7	-124.8	-124.9	-124.8	-128.4	-152.4	-128.0	-125.0	-137.0	-137.0
0.32	-120.2	-121.8	-120.4	-121.9	-122.4	-146.4	-125.0	-122.0	-137.0	-137.0
0.50	-117.3	-120.1	-117.2	-120.0	-118.5	-142.5	-123.0	-120.1	-137.0	-137.0
1.00	-111.8	-117.0	-111.8	-117.0	-112.5	-136.5	-120.0	-117.0	-137.0	-137.0

号光强,使散粒噪声的影响受到限制;带宽需满足50~250 kHz的信号频段;信号频段内需具有20 dB以上的共模抑制比,使RIN得到有效抑制;至少具有 $10^5$ 量级增益,且第一级跨阻放大作为主增益级,使电学噪声保持在远小于光散粒噪声的水平。

## 2.2 电路原理

针对悬浮光力系统的需求,本文设计的QPD探测电路方案如图3所示,通过有源电流滤波将光电流的直流分量和交流分量分解后,分别经跨阻放大电路转换且放大为电压信号,四个象限和参考信号均采用相同的电路对光电流进行处理。图中, $V_A$ 、 $V_B$ 、 $V_C$ 、 $V_D$ 为对应象限光电流的交流分量转换的交流电压信号,用以提取微粒的三轴位移信息<sup>[23]</sup>, $V_{AD}$ 、 $V_{BD}$ 、 $V_{CD}$ 和 $V_{DD}$ 为

光电流直流分量转换的直流电压信号,用于指示QPD入射光斑的位置, $V_{REF}$ 为参考信号的交流分量转换的交流电压信号, $V_{REFD}$ 为参考信号的直流分量转换的直流电压信号。

电流滤波方案针对QPD芯片结构设计,其优点在于:直流跨阻和交流跨阻增益独立,交流跨阻增益不受直流分量限制;相比BPD中常用的无源电流隔直方案<sup>[27-28]</sup>,该方案使QPD芯片的偏置电压不随光电流变化而变化,从而不影响结电容参数,有利于保持QPD象限间响应的一致性。本文选用滨松光子G6849型号的QPD芯片,实测在1064 nm处的响应度为0.55 A/W,饱和光功率大于40 mW。

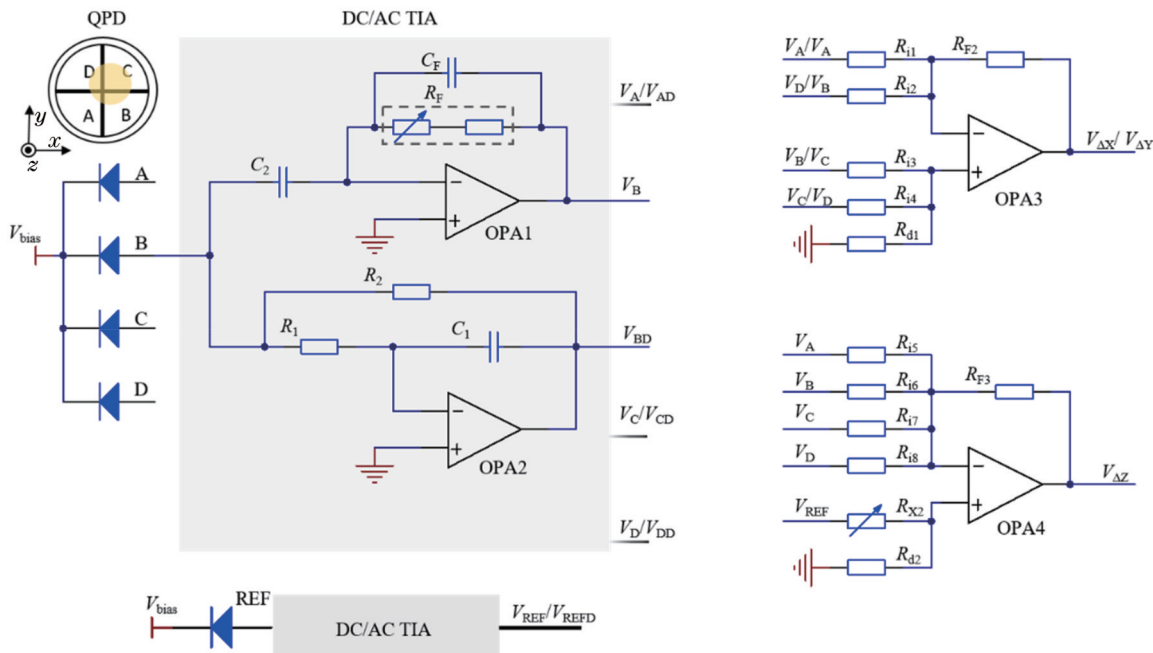


图3 四象限探测器的电路原理图  
Fig. 3 Schematic of the quadrant photodetector

## 2.3 四象限响应系数校准

图3所示的QPD探测电路方案,在X、Y轴方向上,通过象限间的减法运算实现共模抑制,在Z轴方向上,通过引入参考信号做减法运算实现共模抑制,因此各象限及参考信号的响应系数差异会直接影响共模抑制的效果。相比BPD只有单路跨阻放大结构,QPD具有四路跨阻放大结构,需要对各象限的响应系数校准,才能获得较好的共模抑制比。由图1(c)的噪声模型可知,跨阻放大电路的输出响应受光电二极管及电子元器件的参数影响<sup>[26]</sup>。

QPD芯片的响应度 $\eta$ 影响信号的增益,结电容 $C_D$ 影响信号的相位。本文通过调节光路中QPD的入射光斑位置校准象限间响应度 $\eta$ 的差异,通过调节QPD芯片偏置电压并在不同偏压下对结电容进行测量,提

高象限间结电容参数的匹配度。QPD芯片各象限结电容的测量方法如下:在遮光条件下将QPD各象限分别接入同一跨阻放大电路,对跨阻放大器的正相输入端施加扫频激励信号,测量各象限反馈系数的实际响应曲线,再通过理论计算<sup>[26]</sup>采用最小二乘法拟合出各象限在不同偏压下的结电容值,最终将QPD象限间结电容差异校准到1%以内。

四象限响应一致性要求QPD各象限在电路设计上保持高度匹配,主要受电阻和电容的精度、稳定性影响,尤其是跨阻反馈电阻 $R_F$ 的影响。所以图3中的电路均选用高精度、低温漂的精密电阻和电容。但 $R_F$ 的阻值在100 kΩ量级,即使选用精密电阻也存在阻值误差,因此采用可调电位器串联高精度固定阻值电阻的方式形成跨阻反馈电阻 $R_F$ ,并通过测试输出响应曲线校准电阻阻值误差。象限间增益和相位在校准前后的

差异对比如图4(a)所示,在50~250 kHz探测信号频段内,象限间增益差异小于0.04%,相位差异小于

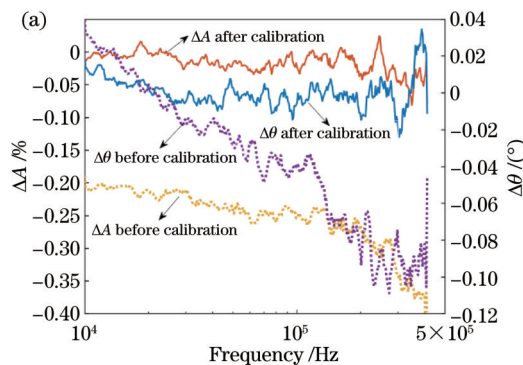


图4 QPD四象限响应校准效果。(a)象限间增益和相位校准前后的差异对比;

Fig. 4 Response calibration results of four quadrants of QPD. (a) Comparison of gain and phase differences between quadrants before and after calibration; (b) baud diagram of the frequency response of the trans-resistance circuit in each quadrant

### 3 分析与讨论

如图1所示,基于QPD的悬浮光力探测系统与基于BPD的探测系统相比,前者的系统更为简单:1064 nm激光束经过声光调制器(AOM)加压衍射,通过分束器分成两束,一束作为QPD的参考光,另一束经物镜高度会聚形成光阱捕获微粒,微粒的散射光与捕获光干涉形成带有微粒位置信息的探测光,非球面透镜采集探测光经聚焦透镜进入QPD光敏面,检测微粒的运动信息。三个方向的运动信号分别被传送到锁相放大器以产生冷却反馈信号,反馈信号的总和驱动AOM进行激光功率调制。

QPD在悬浮光力探测系统中的共模抑制性能测试。悬浮光力系统中纳米微粒的谐振频率一般在50~250 kHz之间,利用信号源控制AOM在该频率范围内对光源进行调制。图5(a)为三轴对200 kHz信号共模抑制后的时域图,图5(b)为三轴在不同频率下测试得

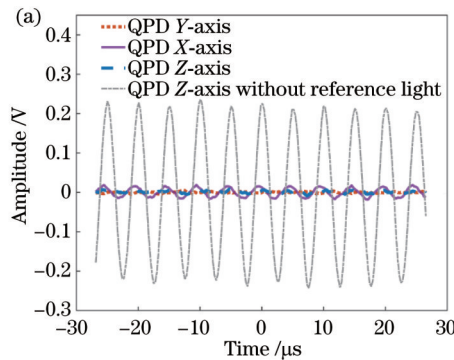
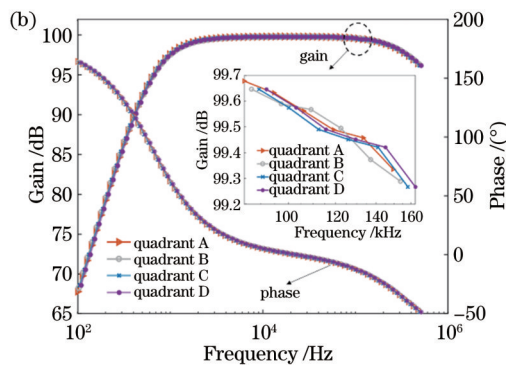


图5 QPD在悬浮光力探测系统中的共模抑制效果。(a) QPD对200 kHz信号共模抑制后的时域图;

Fig. 5 Common mode rejection effect diagram of the triaxial output of the QPD. (a) Time domain diagram of common mode rejection for 200 kHz signal; (b) CMRR measured at different frequencies

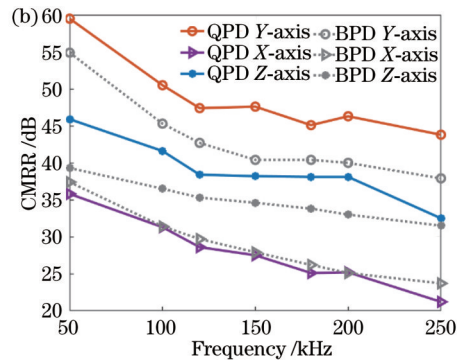
在悬浮光力系统实际应用中,如对仄牛量级的极弱力测量中,要求探测器在测量带宽上保持只受散粒

0.02°,经过校准,各象限跨阻电路频率响应的波特图如图4(b)所示。



到的共模抑制比,并且在同样条件下测试了PDB450C-AC型平衡探测器的共模抑制比进行对比。测试结果表明,QPD的Y轴、Z轴的共模抑制效果优于PDB450C-AC,X轴的效果(100~200 kHz)与之相当。

QPD和BPD三轴的共模抑制效果均存在差异:Y轴效果最佳,在测试频段内均优于45 dB;X轴效果最差,相比Y轴差20 dB以上。针对X轴和Y轴的共模抑制效果差异,将QPD相对光路逆时针旋转90°后重新测量,此时X轴硬件通道的共模抑制比得到很大提升,因此X轴和Y轴共模抑制比差异与QPD硬件无关,猜测是AOM中声波渡越时间引起X轴(与声波传播方向同向)光相位差异,导致共模抑制效果较差。Z轴的参考光不经过真空腔,路径与探测光存在较大差异,且参考光入射的光电二极管在参数上与QPD光电二极管不完全一致,所以Z轴的共模抑制效果无法达到Y轴的水平。



噪声限制的性能。因此在不同入射光功率下,测试了QPD在悬浮光力探测系统中的噪声性能,并对噪声信

号进行1/3倍频程分析和噪声拟合,测试和拟合结果如图6所示。由图6可知,当总入射光功率小于12 mW时,X轴和Y轴的噪声性能相近,且优于Z轴,随着入射光功率继续增加,X轴的噪声功率谱密度快

速上升,最终超过Y轴和Z轴。分析原因如下:Z轴由于参考光的引入,散粒噪声较大,在低光功率下散粒噪声占主导,故噪声较高;X轴共模抑制比最差,在高光功率下RIN占主导,故噪声超过Y轴和Z轴。

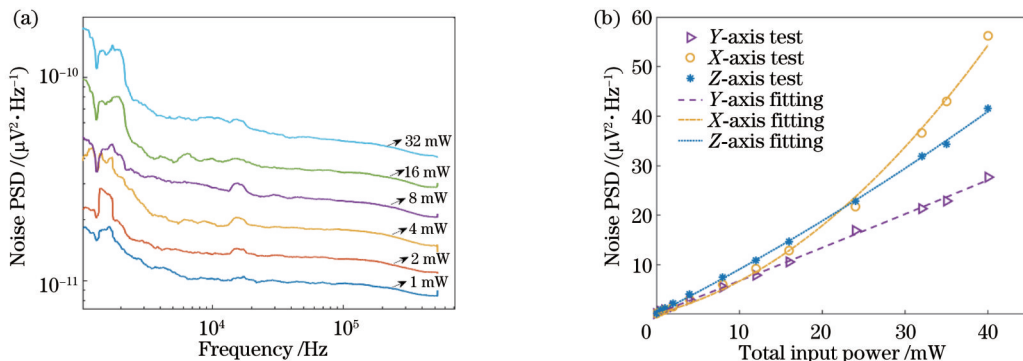


图6 QPD在不同总入射光功率下的噪声功率谱密度。(a) Y轴测试结果;(b)三轴噪声拟合

Fig. 6 Noise PSD of QPD at different input optical powers. (a) Test results of Y-axis; (b) three axes noise fitting

表2 由拟合结果得到的QPD探测系统在不同入射光功率下的噪声分解

Table 2 Noise decomposition of QPD detection system at different input optical powers obtained from fitting results

$\overline{P}_{\text{all}}/\text{mW}$	Test $D_n/(\text{dBV}^2 \cdot \text{Hz}^{-1})$	Fitting $D_n/(\text{dBV}^2 \cdot \text{Hz}^{-1})$	Fitting $D_{\text{RIN}}/(\text{dBV}^2 \cdot \text{Hz}^{-1})$	Fitting $D_{\text{shot}}/(\text{dBV}^2 \cdot \text{Hz}^{-1})$	Fitting $D_e/(\text{dBV}^2 \cdot \text{Hz}^{-1})$
0	-129.4	-129.4	0	0	-129.4
1	-120.6	-121.1	-153.7	-121.8	-129.4
2	-118.2	-118.4	-147.7	-118.8	-129.4
4	-115.4	-115.6	-141.6	-115.8	-129.4
8	-112.6	-112.7	-135.6	-112.8	-129.4
16	-109.8	-109.7	-129.6	-109.8	-129.4
32	-106.7	-106.7	-123.6	-106.8	-129.4
40	-105.6	-105.7	-121.6	-105.8	-129.4

悬浮光力探测系统的Y轴方向不受AOM渡越时间和参考光的影响,能充分体现QPD的性能,所以根据拟合结果对Y轴输出实现噪声分解,结果如表2所示,表中 $\overline{P}_{\text{all}}$ 为QPD总平均入射光功率。由表2可知,在1~40 mW入射光功率范围内, $D_{\text{RIN}}$ 低于 $D_{\text{shot}}$ 15 dB以上,RIN得到有效抑制,且电学噪声远低于散粒噪声基准,QPD总体噪声性能只由散粒噪声主导。QPD的输出涉及四路跨阻电路和减法运算电路,因此在相同增益下,即使克服电流差分设计难点,其理论电学噪声功率谱密度极限仍是BPD的4倍(6 dB)以上。与表1商用BPD的噪声分解结果相比,本文设计的QPD电学噪声功率谱密度较商用BPD高7.6 dB,仅比理论极限高1.6 dB。对比差分探测时相同总入射光功率下的 $D_{\text{RIN}}$ ,QPD对RIN的抑制效果更好,且具有更高的饱和光功率,可以限制散粒噪声影响,因此其性能足以满足悬浮光力系统的探测要求。

## 4 结 论

为了改善基于QPD方案的悬浮光力系统探测性

能,本文设计了一种QPD有源电流滤波方案,在不影响QPD结电容的同时,将光电流的直流分量和交流分量分解,实现 $10^5$ 量级单级跨阻放大,优化了探测器的电学噪声,并校准了四象限响应系数。结果表明在50~250 kHz信号频段内,QPD的最佳共模抑制效果均优于45 dB,在1~40 mW入射光功率范围内,QPD达到只受散粒噪声限制的噪声性能。本文设计的QPD已成功应用于悬浮光力系统的力学量传感<sup>[25]</sup>,为构建高性能、小型化的探测方案奠定了基础。在未来的工作中,可以在QPD电路中加入延时校正模块,校正AOM引入的延时,从而充分发挥QPD的共模抑制性能。

## 参 考 文 献

- [1] 李银妹,龚雷,李迪,等.光镊技术的研究现况[J].中国激光,2015,42(1):0101001.  
Li Y M, Gong L, Li D, et al. Progress in optical tweezers technology[J]. Chinese Journal of Lasers, 2015, 42(1): 0101001.
- [2] 韩翔,陈鑫麟,熊威,等.真空光镊系统及其在精密测量中的研究进展[J].中国激光,2021,48(4):0401011.  
Han X, Chen X L, Xiong W, et al. Vacuum optical tweezers system and its research progress in precision measurement[J].

- Chinese Journal of Lasers, 2021, 48(4): 0401011.
- [3] Gieseler J, Novotny L, Quidant R. Thermal nonlinearities in a nanomechanical oscillator[J]. Nature Physics, 2013, 9(12): 806-810.
- [4] Kuhn S, Stickler B A, Kosloff A, et al. Optically driven ultra-stable nanomechanical rotor[J]. Nature Communications, 2017, 8(1): 1-5.
- [5] Moore D C, Geraci A A. Searching for new physics using optically levitated sensors[J]. Quantum Science and Technology, 2021, 6(1): 014008.
- [6] Tebbenjohanns F, Frimmen M, Jain V, et al. Motional sideband asymmetry of a nanoparticle optically levitated in free space[J]. Physical Review Letters, 2020, 124(1): 013603.
- [7] Blakemore C P, Rider A D, Roy S, et al. Three-dimensional force-field microscopy with optically levitated microspheres[J]. Physical Review A, 2019, 99(2): 023816.
- [8] Kawasaki A, Fieguth A, Priel N, et al. High sensitivity, levitated microsphere apparatus for short-distance force measurements[J]. The Review of Scientific Instruments, 2020, 91(8): 083201.
- [9] Monteiro F, Li W Q, Afek G, et al. Force and acceleration sensing with optically levitated nanogram masses at microkelvin temperatures[J]. Physical Review A, 2020, 101(5): 053835.
- [10] Ranjit G, Cunningham M, Casey K, et al. Zeptonewton force sensing with nanospheres in an optical lattice[J]. Physical Review A, 2016, 93(5): 053801.
- [11] Monteiro F, Ghosh S, Fine A G, et al. Optical levitation of 10- $\mu$ m spheres with nano-g acceleration sensitivity[J]. Physical Review A, 2017, 96(6): 063841.
- [12] Xiong F, Yin P R, Wu T, et al. Lens-free optical detection of thermal motion of a submillimeter sphere diamagnetically levitated in high vacuum[J]. Physical Review Applied, 2021, 16: L011003.
- [13] Armata F, Latminal L, Plato A D K, et al. Quantum limits to gravity estimation with optomechanics[J]. Physical Review A, 2017, 96(4): 043824.
- [14] Hebestreit E, Frimmen M, Reimann R, et al. Sensing static forces with free-falling nanoparticles[J]. Physical Review Letters, 2018, 121(6): 063602.
- [15] 郑瑜. 真空光镊及其反馈控制[D]. 合肥: 中国科学技术大学, 2019.
- Zheng Y. Feedback control of the optical levitation in vacuum [D]. Hefei: University of Science and Technology of China, 2019.
- [16] Delić U, Reisenbauer M, Dare K H, et al. Cooling of a levitated nanoparticle to the motional quantum ground state[J]. Science, 2020, 367(6480): 892-895.
- [17] Magrini L, Rosenzweig P, Bach C, et al. Real-time optimal quantum control of mechanical motion at room temperature[J]. Nature, 2021, 595(7867): 373-377.
- [18] Tebbenjohanns F, Mattana M L, Rossi M, et al. Quantum control of a nanoparticle optically levitated in cryogenic free space [J]. Nature, 2021, 595(7867): 378-382.
- [19] Tischer C, Pralle A, Florin E L. Determination and correction of position detection nonlinearity in single particle tracking and three-dimensional scanning probe microscopy[J]. Microscopy and Microanalysis, 2004, 10(4): 425-434.
- [20] Ranjit G, Atherton D P, Stutz J H, et al. Attoneutron force detection using microspheres in a dual-beam optical trap in high vacuum[J]. Physical Review A, 2015, 91(5): 051805.
- [21] Millen J, Deesawan T, Barker P, et al. Nanoscale temperature measurements using non-equilibrium Brownian dynamics of a levitated nanosphere[J]. Nature Nanotechnology, 2014, 9(6): 425-429.
- [22] Xiong W, Xiao G Z, Han X, et al. Back-focal-plane displacement detection using side-scattered light in dual-beam fiber-optic traps[J]. Optics Express, 2017, 25(8): 9449-9457.
- [23] Hebestreit E. Thermal properties of levitated nanoparticles[D]. Zurich: ETH Zurich, 2017.
- [24] Vijayan J, Zhang Z, Piotrowski J, et al. Scalable all-optical cold damping of levitated nanoparticles[J]. Nature Nanotechnology, 2023, 18(1): 49-54.
- [25] Liang T, Zhu S C, He P T, et al. Yoctonewton force detection based on optically levitated oscillator[J]. Fundamental Research, 2023, 3(1): 57-62.
- [26] 杰拉尔德·格雷姆. 光电二极管及其放大电路设计[M]. 赖康生, 许祖茂, 王晓旭, 译. 北京: 科学出版社, 2012: 41, 92, 113.
- Graeme J. Photodiode amplifiers: OP AMP solutions[M]. Lai K S, Xu Z M, Wang X X, Transl. Beijing: Science Press, 2012: 41, 92, 113.
- [27] 王金晶, 贾晓军, 彭堃墀. 平衡零拍探测器的改进[J]. 光学学报, 2012, 32(1): 0127001.
- Wang J J, Jia X J, Peng K C. Improvement of balanced homodyne detector[J]. Acta Optica Sinica, 2012, 32(1): 0127001.
- [28] 斯晓丽. ~kHz量级平衡零拍探测器的研究[J]. 激光与光电子学进展, 2021, 58(9): 0927003.
- Jin X L. Study on kHz balanced homodyne detector[J]. Laser & Optoelectronics Progress, 2021, 58(9): 0927003.

## A Low-Noise Quadrant Photodetector for Levitated Optomechanical Systems

Wang Yingying<sup>1</sup>, He Peitong<sup>1</sup>, Liang Tao<sup>1</sup>, Gao Xiaowen<sup>1\*</sup>, Jiang Jing<sup>2</sup>, Chen Xingfan<sup>2</sup>,  
Hu Huizhu<sup>1,2\*\*</sup>

<sup>1</sup>Research Center for Quantum Sensing, Zhejiang Lab, Hangzhou 310023, Zhejiang, China;

<sup>2</sup>College of Optical Science and Engineering, Zhejiang University, Hangzhou 310027, Zhejiang, China

### Abstract

**Objective** Due to the excellent detection performance, levitated optomechanical systems have become intriguing in the field of precision measurement. The detection schemes of such systems mainly contain the balanced photodetector (BPD) and quadrant photodetector (QPD). The BPD has a current differential structure that can eliminate common-mode DC

signals, which results in extra low noise. However, the BPD scheme has the disadvantage of complicated detection systems because one BPD usually measures the particle displacement in one direction. In contrast, a QPD can simultaneously detect displacements in three directions, which effectively simplifies the detection system. Usually, QPDs amplify not only the AC photocurrent generated by the fluctuations of the incident optical power, which mainly arise from the displacements to be measured, but also the DC photocurrent corresponding to the average incident optical power. As a consequence, QPDs always show worse noise performance than BPDs. Therefore, this work proposes a QPD scheme, which reduces the electrical noise of a QPD through electrical filtering and achieves a common-mode rejection ratio (CMRR) as high as possible, and the response coefficients of the four quadrants are calibrated. The QPD is a promising alternative scheme to the BPD, which has high detection sensitivity and is beneficial to the miniaturization of levitated optomechanical systems.

**Methods** This work proposes a QPD scheme by building the noise model in levitated optomechanical systems, according to which the proportions of electrical noise, optical shot noise, and relative intensity noise (RIN) can be obtained. A current filter circuit is built with an operational amplifier, and the DC and AC components of the photocurrent are separated without any influence on the junction capacitance of the QPD sensor. As a result, the AC transimpedance gain is free from the limitation of the DC component, and meanwhile, the electrical noise is reduced. The converted voltage signal from the AC component is used to demodulate the three-axis displacement information of the particle, and that converted from the DC component is used to indicate the position of the incident light on the QPD. Moreover, a QPD sensor with high saturated optical power is used to suppress the shot noise to the maximum extent. In addition, the bias voltage of the QPD sensor is adjusted to reduce the junction capacitance differences between the four quadrants, and the feedback resistance of each quadrant is calibrated through the connection of an adjustable potentiometer in series with a high-precision fixed resistance resistor. Consequently, the response coefficients of four quadrants are unified, and the CMRR of the detector is improved to a large degree.

**Results and Discussions** Attributed to the calibration of the response coefficients, the junction capacitance difference between QPD quadrants is less than 1%, the circuit gain difference is less than 0.04%, and the phase difference is less than 0.02° (Fig. 4). The CMRR and noise performance of the QPD are tested in a levitated optomechanical system and are compared with those of a commercial BPD which meets the requirements of such a system with superior noise performance. The results show that the power spectral density (PSD) of the electrical noise of the QPD is  $-129.4 \text{ dBV}^2/\text{Hz}$  with a circuit gain of  $10^5$  and reaches the same level as that of the commercial BPD (Tables 1 and 2). The CMRR of QPD is greater than 45 dB (50–250 kHz), which is better than that of the commercial BPD [Fig. 5(b)]. When the incident optical power is in the range of 1–40 mW, the noise performance of the QPD is only limited by shot noise (Fig. 6, Table 2). Overall, compared with the commercial BPD, the QPD proposed in this work can better suppress RIN and has higher saturated optical power to effectively limit the influence of shot noise. Therefore, the detection performance of the proposed QPD can meet the requirements of levitated optomechanical systems.

**Conclusions** An active current filtering scheme with operational amplifiers is designed in this work to improve the detection performance of the QPD-based levitated optomechanical system. A  $10^5$  single-stage transimpedance gain is achieved so that the electrical noise is optimized. The response coefficients of four quadrants are calibrated so that the CMRR is improved, which is greater than 45 dB in the frequency range of 50–250 kHz. When the incident optical power is in the range of 1–40 mW, the noise performance of the QPD is only limited by shot noise. The QPD scheme has been successfully applied for extremely weak force sensing in levitated optomechanical systems, which lays the foundation for the high-performance, miniaturized detection system. In the future, the delay introduced by the acoustic-optic modulator can be compensated with a calibration module, so as to further improve the common-mode rejection performance of the QPD scheme.

**Key words** detectors; photodetectors; levitated optomechanical system; noise decomposition; common mode rejection